Cancer Letters 452 (2019) 38–50

Contents lists available at ScienceDirect

Cancer Letters

journal homepage: www.elsevier.com/locate/canlet

Original Articles

Tumor targeting and microenvironment-responsive multifunctional fusion protein for pro-apoptotic peptide delivery

Jun Yin[1], Dingkang Liu[1], Lichen Bao, Qun Wang, Ye Chen, Shan Hou, Yali Yue, Wenbing Yao**, Xiangdong Gao*

Jiangsu Key Laboratory of Druggability of Biopharmaceuticals and State Key Laboratory of Natural Medicines, School of Life Science and Technology, China Pharmaceutical University, Nanjing, 210009, China

ARTICLE INFO

Keywords:
Polypeptide
Matrix metalloproteinase 2
Targeted therapy
Anticancer peptide

ABSTRACT

The great therapeutic potential of peptides has not yet been achieved, mainly due to their remarkably short *in vivo* half-life. Although conjugation to macromolecules has been an effective way of improving protein *in vivo* half-life, the steric hindrance of macromolecules usually reduces the *in vivo* efficacy of peptides. Here we report a complex delivery system made from PsTag polypeptide, polyglutamic acid chain, matrix metalloproteinase 2 (MMP2)-degradable domain and cationic cell penetrating peptide for anticancer peptide delivery. Clear evidence was shown *in vitro* and *in vivo* to demonstrate that this multifunctional protein fusing a pro-apoptotic KLAKL-AKKLAKLAK (KLA), named PAK, can increase circulation time in blood, enhance accumulation at tumor sites, eliminate the PsTag domain and the polyanionic sequence when triggered by tumor overexpressing MMP2, and then expose the cell penetrating peptide to realize the potent cellular uptake of KLA. Treatment of tumor-bearing mice with PAK could markedly induce tumor cells apoptosis and inhibit tumor growth, with no significant adverse effects. These results suggest our fusion protein can be a potential delivery system for peptide delivery in cancer treatments.

1. Introduction

Over the years peptides have evolved as promising therapeutic and diagnostic agents. Currently, there are approximately 60 peptide-based therapeutics on the market and more than 500 therapeutic peptides in preclinical development, with cancer treatment being one of the most explored therapeutic areas [1,2]. Because anticancer peptides have a lower tendency for development of resistance by tumor cells compared to conventional chemotherapies, increasing attention has been paid to peptide-based cancer treatment [3–6]. Anticancer peptides also have many unique advantages, such as small molecular weight, tumor-penetrating ability, low immunogenicity, good biocompatibility, and ease of synthesis and modification [7,8]. Unfortunately, peptides generally have a short *in vivo* half-life, which severely limits their clinical application [9]. Developing anticancer peptides with extended half-life but reduced side effects is still an important part of cancer research.

Pharmacokinetic extension is no longer just a way to create improved second-generation biologicals but plays a vital role for current development of biopharmaceutical drugs. Coupling of polymers such as polyethylene glycol (PEG) to bioactive agents has been proven to be an effective approach for prolonging the *in vivo* half-lives of the agents [10–13]. Moreover, PEGylated drugs possess passive tumor targetability via the enhanced permeability and retention (EPR) effect at tumors [14]. However, PEGylation has several potential safety problems, such as formation of antibodies against polymer itself and the very low degree of biodegradability of the PEG polymer, which can lead to adverse effects, such as vacuolation of the kidney epithelium [15,16]. To circumvent these problems, PsTag polypeptides have been invented. These uncharged and unstructured hydrophilic, biodegradable amino acid sequences can be fused to biomolecules using recombinant DNA technology and can reduce the rapid kidney clearance in a similar approach to PEG, based on an increased hydrodynamic radius [17–19]. However, they still do not solve the problems of the steric hindrance of macromolecules, which particularly influences the bioactivity of peptides.

One way to eliminate steric hindrances and decrease adverse effects is to exploit an inactive prodrug that is specifically activated at the tumor site. It is well known that tumor cells can remodel the tumor

* Corresponding author.
** Corresponding author.
E-mail addresses: wbyao@cpu.edu.cn (W. Yao), xdgao@cpu.edu.cn (X. Gao).
[1] These authors contributed equally to this work.

https://doi.org/10.1016/j.canlet.2019.03.016
Received 5 November 2018; Received in revised form 6 March 2019; Accepted 8 March 2019

microenvironment, which in turn can further influence the behavior and state of tumor cells [20,21]. There is a significant difference between the microenvironment of tumor cells and normal cells, such as abnormal blood vessels, oxidation, perfusion, pH and metabolic status [22,23]. Matrix metalloproteinase 2 (MMP2), which plays a significant role in extracellular matrix (ECM) degradation, promotes tumor cells to migrate out of the primary tumor to form metastases [24–26]. Due to the high expression of MMP2 at almost all tumors, it is possible to design a prodrug that can be specifically activated to destroy tumor cells through introducing a cleavage site of MMP2 [27–29].

The goal of this work was to develop a general strategy that combined the aforementioned features to produce powerful therapeutic drugs for cancer therapy.

To test this strategy, we employed a typical cationic amphipathic peptide, KLAKLAKKLAKLAK (KLA) [30,31]. After internalization of KLA into the eukaryotic cell, disruption of the mitochondrial membrane was triggered, which resulted in leakage of cytochrome c and induction of cell apoptosis [32]. To elevate cell uptake efficiency, KLA was fused with several cationic cell-penetrating peptides (CPPs), such as polyarginine and Tat peptides [33,34]. Although the uptake efficiency of CPP-KLA was significantly increased, there were two weaknesses of CPP-KLA use as a drug: its short half-life and poor tumor selectivity. In addition, due to the antimicrobial activity of KLA, expression and purification as recombinant peptides in prokaryocyte expression systems were considered to be almost impossible.

Therefore, we designed a multifunctional fusion protein, named PAK, that includes (1) PsTag for enhanced circulation time in the blood, deactivation of KLA and passive tumor targetability via the EPR effect; (2) a polyanionic sequence to neutralize CPP; (3) a sensitive cleavage sequence of MMP2 for specific activation at tumor sites; (4) a CPP to deliver KLA into the cells and (5) KLA as cytostatic/cytotoxic component (Fig. 1). Deactivation was crucial not only for bioactivity but also for the production in *Escherichia coli (E. coli)*, because active KLA was too toxic for *E. coli* cells to be acquired. Here, we demonstrated that the genetic fusion of this protein to a model peptide enhanced delivery to the tumor, minimized the nonspecific toxic effect and improved the pharmacokinetic properties without compromising its anticancer activity. These findings showed that our method had potential to greatly advance the therapeutic applications of peptides.

2. Materials and methods

2.1. Construction of expression plasmids and preparation of the molecules

The DNA coding sequence of the complete fusion protein PAK contained the following components: a PsTag polymer of 216 amino acids, a polyglutamic acid chain of 8 negatively charged amino acids (the neutralizing part of CPP), a sequence of MMP2 cleavage site (PLGLAG), a positive charge CPP of 8 arginine, and a KLA domain with cytostatic activity followed by one cysteine residue, which is the only cysteine in the entire sequence. Based on the PAK sequence, the coding sequence of the control fusion protein PK replaced the MMP2 cleavage site with flexible linker GGGGS. The coding sequences of PAK and PK were synthesized by GenScript (Nanjing, China) (Table S1). The two genes were digested with restriction enzymes *Bam*H I and *Hin*d III and ligated into the expression vector pET28a (+), generating pET28a-PAK and pET28a-PK. Then, the two constructs were maintained in *E. coli* Top10 with kanamycin as selection pressure for subsequent expression in *E. coli* BL21 (DE3).

The recombinant *E. coli* strains were cultured in LB medium with 1% kanamycin (100 μg/mL), and the cells were grown at 37 °C until OD_{600} reached approximately 1.0. Then, IPTG (Sigma-Aldrich, St. Louis, MO, USA) was added to the medium to a final concentration of 0.6 mg/L, and cells were cultured at 37 °C for an additional 8 h. The supernatant was collected after ultrasonic crushing of the cells, and the protein was purified using a Q anion exchange resin (GE Healthcare, Pittsburgh, PA, USA), followed by an additional Ni^{2+} affinity chromatography (GE Healthcare, Pittsburgh, PA, USA). Expression levels of each recombinant protein were analyzed by SDS-PAGE (12%) and Western blot. The Western blot was probed with a mouse anti-His-Tag antibody (1:1000 dilutions; GenScript, Nanjing, China) as the primary antibody and HRP-conjugated goat anti-mouse Ig antibody (1:5000 dilutions, GenScript, Nanjing, China) as the secondary antibody. The protein concentration was determined using the Bradford Protein Assay Kit (Thermo Fisher, Massachusetts, USA).

High purity (> 90%) peptides were obtained from GL Biochem Inc. (Shanghai, China). The amino acid sequence of peptides was as follows: R_8-KLA, RRRRRRRRGG $(KLAKLAK)_2$ and R_8-KLAC, RRRRRRR-RGG$(KLAKLAK)_2$GGC. The two amino acid GG were used as a bridge to impart peptide flexibility and minimize potential steric interactions between the targeting peptide and the proapoptotic peptide.

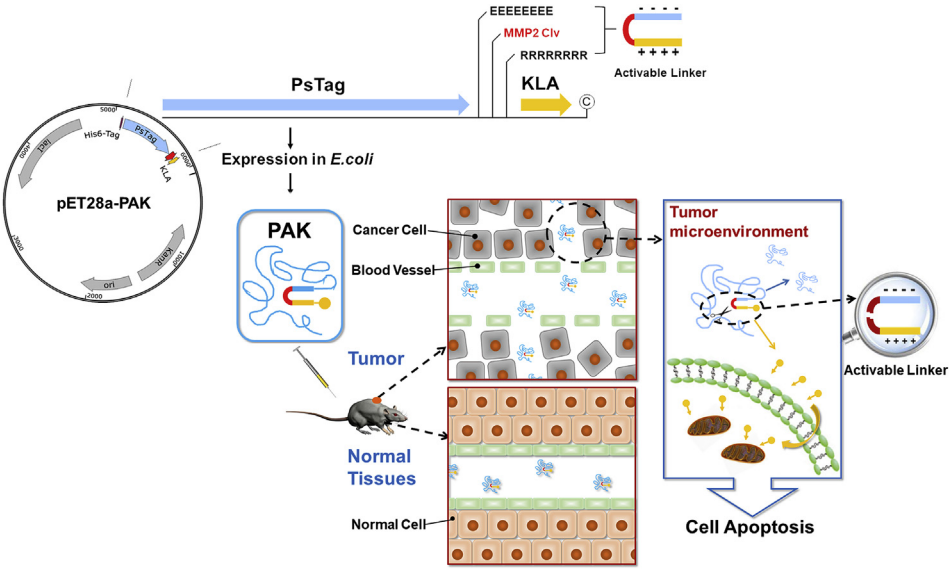

Fig. 1. Construction of the recombinant PAK.
Schematic representation of the DNA/protein sequence of PAK and a summary of its intended functions.

Table 1
Construction of the three molecules.

Molecule	Long-acting domain	Linker	Functional domain
PAK	PsTag216	GGEEEEEEEEPLGLAGRRRRRRRRGG	KLA
PK	PsTag216	GGEEEEEEEEGGGGSRRRRRRRRGG	KLA
R_8-KLA	-	RRRRRRRRGG	KLA

2.2. Characterization of recombinant fusion proteins

Reverse-phase HPLC: The sample solution in PBS was diluted to 5% v/v acetonitrile, 0.065% v/v trifluoroacetic acid (TFA) and 80 μL was subjected to a SepaxGP-C18 column (Sepax Technologies, Inc.) using a high-performance liquid chromatography system (Agilent Technologies, Santa Clara, CA, USA) equipped with an autosampler. The mobile phase consists of two buffers: Buffer A (distilled H_2O, 0.065% TFA) and Buffer B (acetonitrile, 0.065%TFA). The C18 column was first adjusted to an isocratic 5% v/v acetonitrile-water gradient for 10 min, followed by a 5%–60% (v/v) acetonitrile-water gradient over 25 min, at a total solvent flow-rate of 1 mL/min. Absorbance was detected at 219 nm using a UV detector.

Circular dichroism spectra (CD): The CD spectra of proteins (0.1 mg/mL in PBS) were detected by a Jasco-720 spectropolarimeter (Jasco, Groß-Umstadt, Germany) over a wavelength range of 190–260 nm using a 0.2 cm cell.

Mass spectroscopy: The mass spectra of the protein were measured as previously described [17].

Size exclusion chromatography: Analytical SEC of the molecules was measured as previously described [17]. The apparent molecular masses were estimated by interpolation from a calibration line ($R^2 = 0.9991$) (Fig. S1) obtained with the reference proteins thyroglobulin, BSA, ovalbumin, ribonuclease A and vitamin B12 (all from Sepax Technologies, Inc.).

2.3. Enzyme cleavage assay

Proteins were diluted to 0.5 mg/mL in an assay buffer (20 mM Tris, 150 mM NaCl, 10 mM $CaCl_2$, pH 7.5) and placed on ice. The active human recombinant MMP2 (Merck, Darmstadt, Germany) was added to a final concentration of 0.2 ng/μL, and the reaction mixture was cultured at 37 °C. At various time points for up to 8 h, 80 μL aliquots were

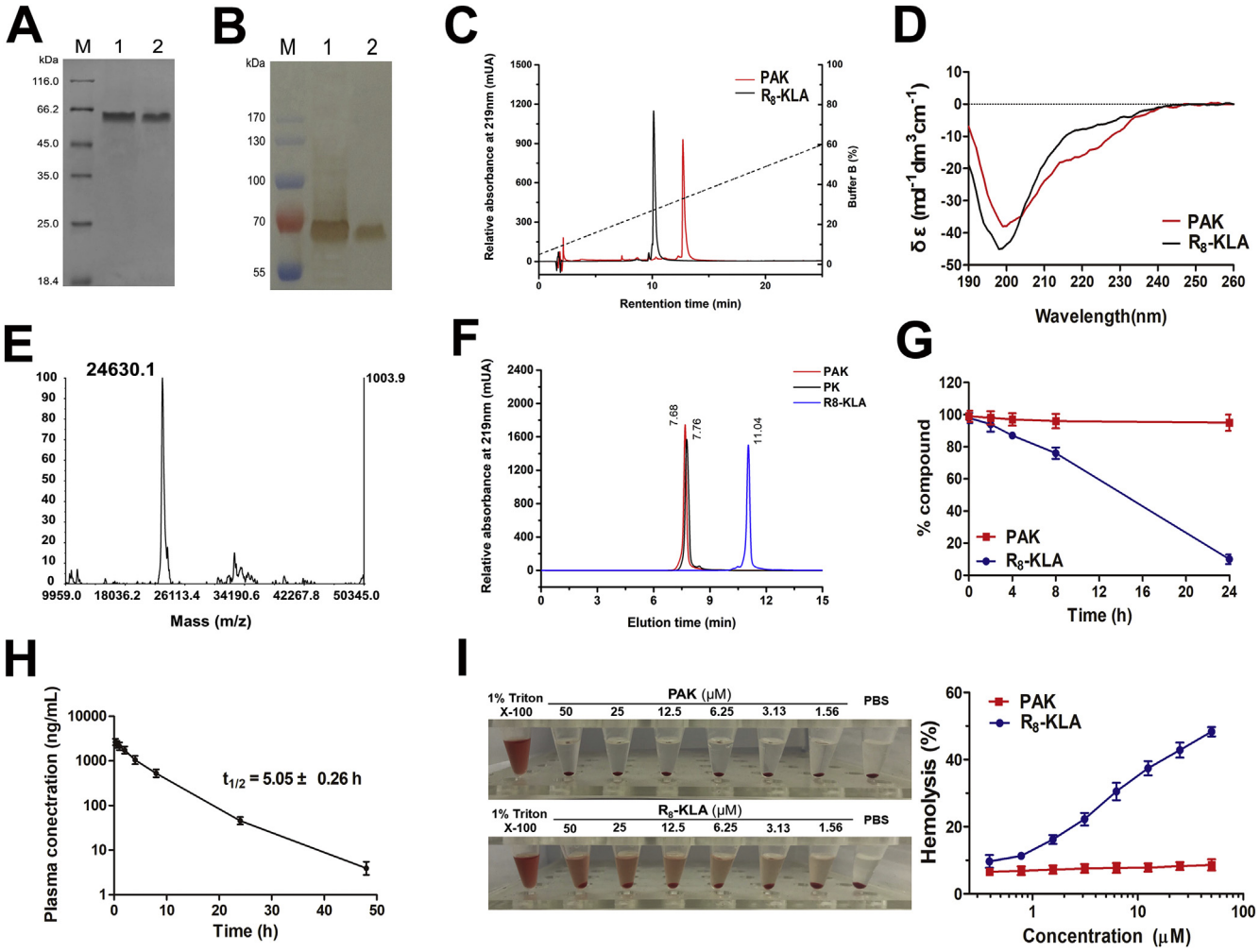

Fig. 2. The characterization of the recombinant fusion proteins.
(A) SDS-PAGE and (B) Western blotting (lane 1: PAK; lane 2: PK) of the recombinant fusion proteins. (C) Purity analysis of PK and PAK by RP-HPLC. (D) Secondary structure of PK and PAK by CD. (E) Absolute molecular weight of PAK by MALDI-TOF mass spectrometry. (F) Hydrodynamic volume of PAK, PK and R_8-KLA by SEC-HPLC. (G) PAK or R_8-KLA was added to serum, and the amounts of PAK and R_8-KLA remaining in serum were quantitated by RP-HPLC at indicated time points. (H) Pharmacokinetic plasma profile of PAK intravenously injected in BALB/c mice (n = 10 per group). (I) Hemolysis assay of PAK and R_8-KLA using BALB/c mouse red blood cells. PBS and Triton X-100 (1%) was used as the negative and positive control, respectively. Data are mean ± SD of three replicates. . (For interpretation of the references to colour in this figure legend, the reader is referred to the Web version of this article.)

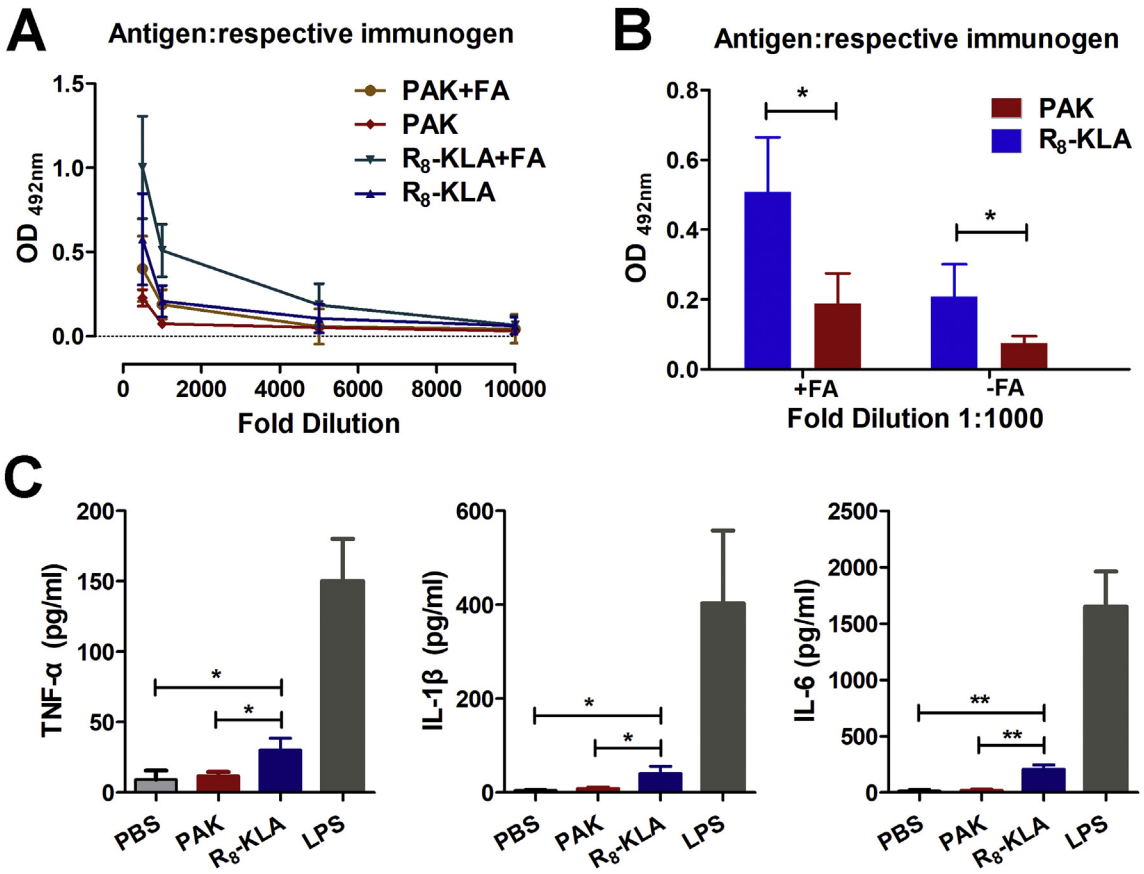

Fig. 3. The immunogenicity of PAK.
(A) Plasma samples were analyzed for immunogenicity according to the protocol given in the Experimental Section (Supplementary Material). Plasma samples were serially diluted (1: 500- 1: 10000). (B) Data was shown for a plasma dilution at 1: 1000. (C) Analysis of cytokine induction in human PBMCs after treatment with PBS, PAK, R_8-KLA or LPS. LPS (10 μg/mL) was used as positive controls. Cytokines that regulate the innate immunity, IL-1β, TNF-α and IL-6, were detected. (Data are means ± SD from n = 6 per group. *$P < 0.05$, **$P < 0.001$).

removed from the reaction wells, immediately mixed 1:4 with SDS gel loading buffer (5 × concentrated), and boiled for 5 min. Samples were subjected to electrophoresis on 15% Urea-SDS-PAGE gels for 90 min at 110 V.

2.4. Cell lines and cultures

A375 (human melanoma cell), HepG2 (human hepatoblastoma cell), MCF7 (human breast cancer cell), BGC823 (human gastric cancer cell) and L02 (human hepatocytes cell) cell lines were obtained from the American Type Culture Collection (ATCC, Manassas, USA) and were cultured in DMEM medium with 10% fetal bovine serum (FBS) and 1% antibiotics (penicillin 100 IU/mL, and streptomycin 100 μg/mL). Cells were cultured at 37 °C with 5% CO_2.

2.5. Cytotoxicity and apoptosis assays

For cytotoxicity assays, cells were seeded in 96-well plates (5,000 cells/well) of complete DMEM supplemented with 10% FBS and incubated at 37 °C. After 12 h, the cells were treated with different concentrations (ranging from 0 to 40 μM) of PAK, PK, or R_8-KLA for 72 h. Then, 10 μL of Cell Counting Kit-8 (CCK-8) solution (MedChemExpress, NJ, USA) was added to each well for 3 h at 37 °C. The sample was measured at 450 nm using a microplate reader (Thermo Fisher, Massachusetts, USA).

To determine the effects of MMP2 on the activity of PAK, the A375 cells were seeded in 96-well plates (5,000 cells/well) at 37 °C. After 12 h, the supernatant was discarded and fresh complete DMEM containing SB-3CT (final concentration 1 μg/mL; MedChemExpress, NJ, USA) and PAK (final concentration ranging from 0 to 40 μM) was added to the cells for 72 h. The L02 cells were seeded in 96-well plates (5,000 cells/well) at 37 °C. After 12 h, the supernatant was discarded and fresh complete DMEM containing the digested product of PAK (final concentration ranging from 0 to 40 μM) was added to the cells for 72 h. The product of digestion was obtained after 4 h of MMP2 enzyme digestion of PAK *in vitro*. Then, 10 μL of CCK-8 solution was added to each well for 3 h at 37 °C. The sample was measured at 450 nm using a microplate reader.

For the analysis of apoptosis, A375 cells were seeded in 6-well plates (50,000 cells/well) of complete DMEM supplemented with 10% FBS and incubated at 37 °C. After 12 h, the cells were incubated with PAK for 72 h at 37 °C. Subsequently, the cells were harvested and washed twice with cold HBSS and then resuspended in 1 × binding buffer at a concentration of 1×10^6 cells/mL. Each 100 μL solution (1×10^5 cells) was incubated with 5 μL of Annexin V-FITC and 5 μL of PI for 15 min at RT in the dark. Then, 400 μL of 1 × binding buffer was added to each sample tube and the apoptotic cells were assessed using a FACSCalibur flow cytometer (BD Bioscience, San Jose, CA, USA).

2.6. Protein of MMP2 in cell lines and detection of apoptotic signaling proteins

To analyze protein of MMP2 in different cell lines, A375, HepG2, MCF7, BGC823 and L02 cell lines were cultured in complete DMEM supplemented with 10% FBS and incubated at 37 °C in a 5% CO_2 atmosphere for 24 h, harvested, and lysed in a RIPA buffer (50 mM Tris

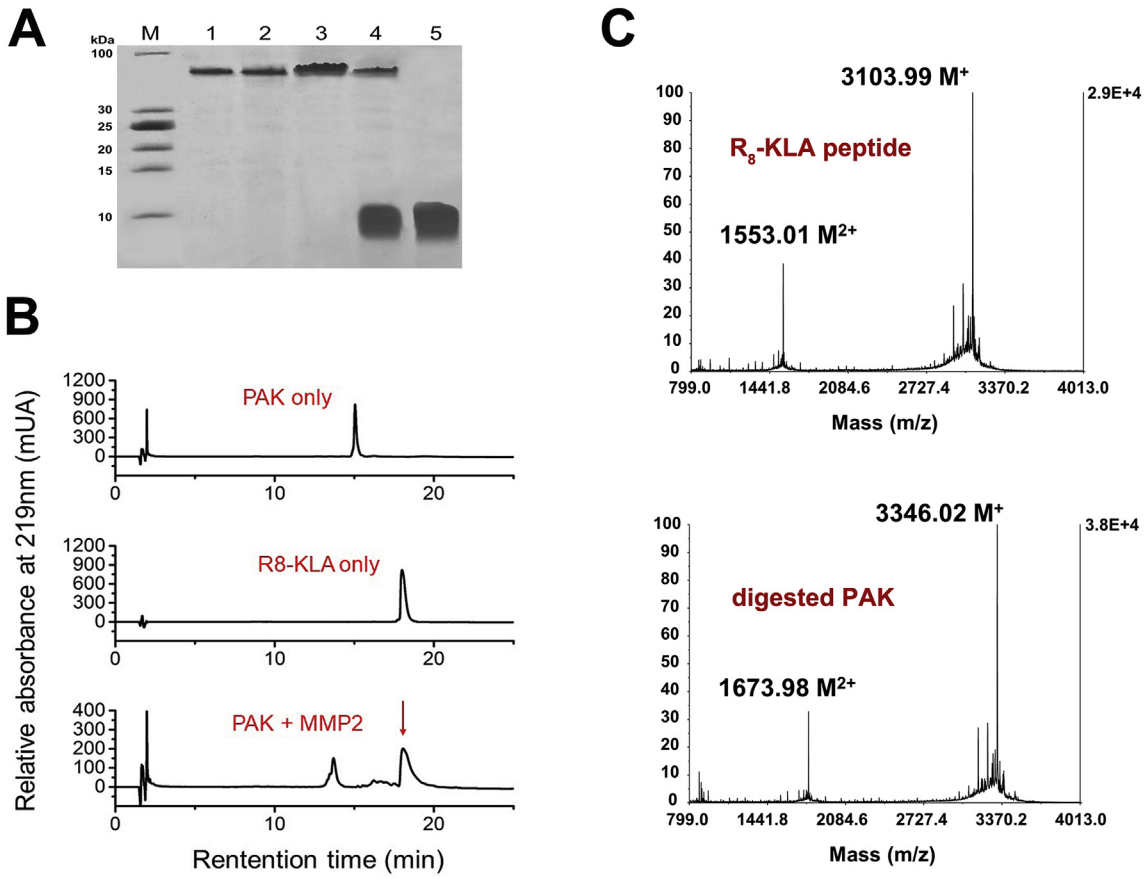

Fig. 4. Enzymatic digestion of PAK by MMP2.
(A) PAK and PK were digested with MMP2 within 4 h at 37 °C and were monitored by Urea-SDS-PAGE (lane 1: PK; lane 2: PK & MMP2; lane 3: PAK; lane 4: PAK & MMP2, lane 5: R_8-KLA). (B) The digestion of PAK was further analyzed by RP-HPLC. (C) Mass spectrometry of R_8-KLA fraction further obtained by preparative HPLC and synthetic R_8-KLA peptide.

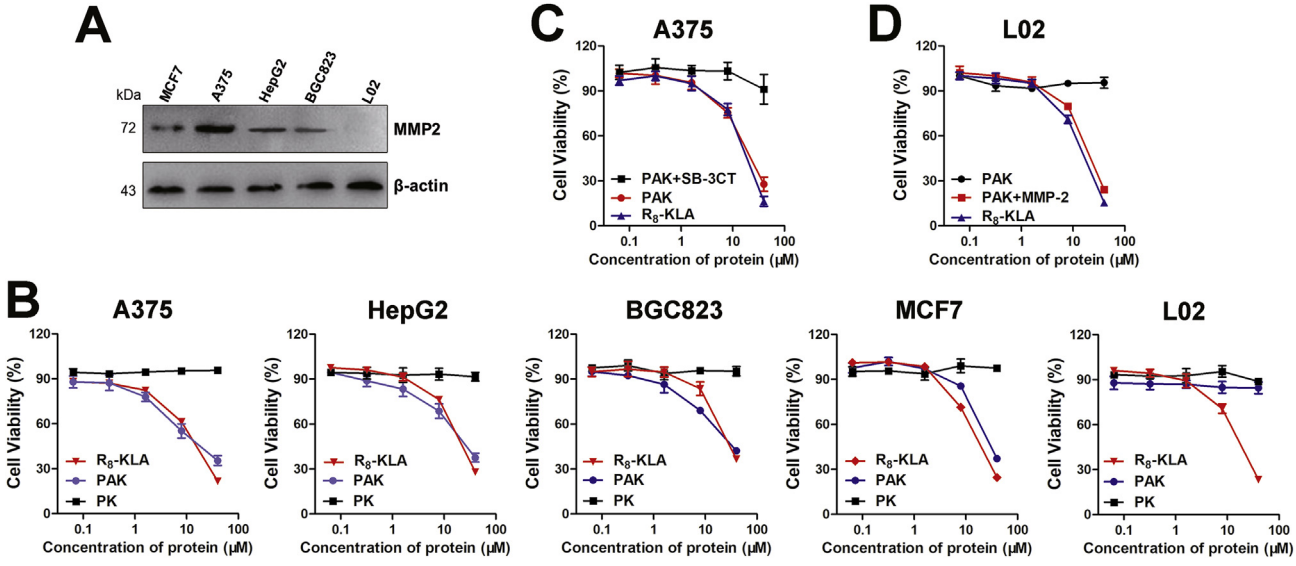

Fig. 5. *In vitro* cytotoxicity of PAK.
(A) Western blot analysis to detect the expression level of MMP2 protein in MCF7, A375, HepG2, BGC823 and L02 cell lines. (B) Selective cytotoxicity of PAK among different cell lines. A375, HepG2, BGC823, MCF7 and L02 cells were treated with indicated products for 72 h at varying concentrations. (C) After pretreatment of SB-3CT, A375 cells were treated with indicated products for 72 h at varying concentrations. (D) L02 cells were treated with indicated products for 72 h at varying concentrations. Data are represented as mean ± SD of three independent experiments.

Table 2
In vitro antitumor effects of the three molecules.

IC_{50} (μM)	Cell Line				
	A375	HepG2	BGC823	MCF7	L02
PAK	11.05 ± 0.73	19.21 ± 0.62	23.92 ± 0.82	25.65 ± 0.86	NA[a]
PK	NA	NA	NA	NA	NA
R_8-KLA	9.76 ± 0.92	14.15 ± 0.36	25.54 ± 0.77	15.70 ± 0.63	14.35 ± 0.74

[a] NA: Not Available. Data are means ± SD of three independent experiments.

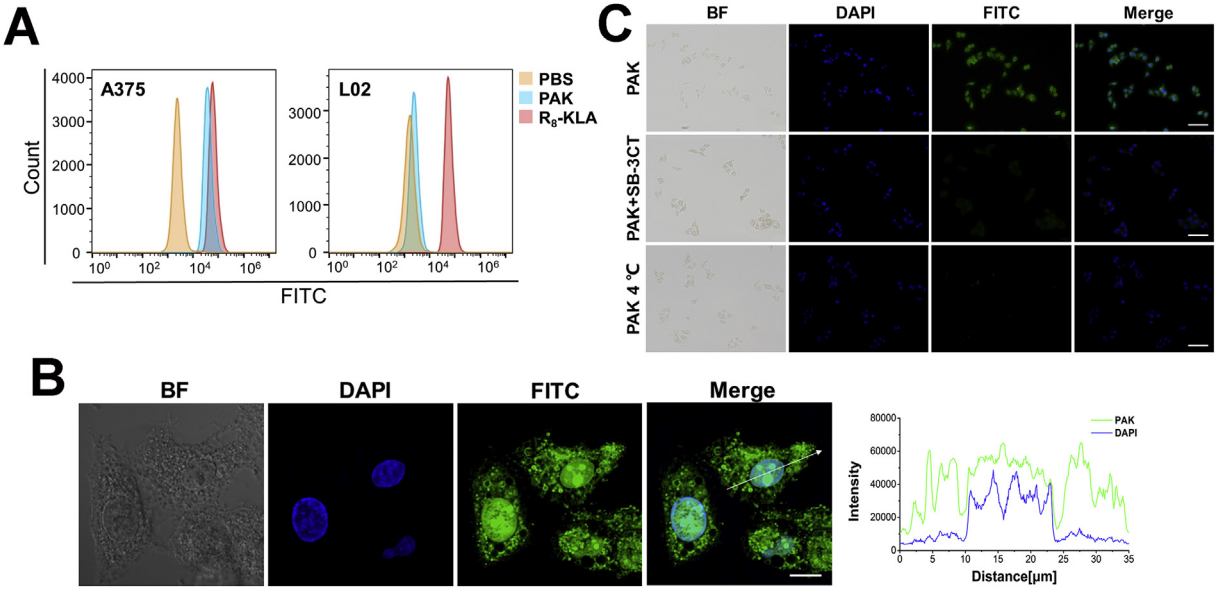

Fig. 6. MMP-dependent cellular uptake of PAK-FITC.
(A) After incubating with FITC-labeled PAK (20 μM) for 48 h, A375 and L02 cells were harvested and subjected to flow cytometry. (B) Confocal fluorescence images and line-scan profiles of fluorescence intensity for A375 cells incubated for 48 h with 20 μM PAK-FITC. Nuclei were stained by DAPI (blue). Scale bars, 20 μm. (C) The fluorescence images of A375 cells after incubation with FITC-labeled PAK (20 μM) under different conditions as indicated. Nuclei were stained by DAPI (blue). Scale bars, 100 μm. . (For interpretation of the references to colour in this figure legend, the reader is referred to the Web version of this article.)

(pH 7.4), 150 mM NaCl, 1%NP-40, 0.25% sodium deoxycholate, 10 mM sodium pyrophosphate, 100 mM sodium fluoride, and 2 mM phenylmethylsulfonyl fluoride) with protease inhibitors (Sigma-Aldrich, St. Louis, MO, USA). Subsequently, the total cell proteins were electrophoresed in a 10% SDS-PAGE followed by transfer to polyvinylidene difluoride (PVDF) membrane (Millipore, Bedford, MA, USA). After blocking with 5% (w/v) nonfat dry milk, the blots were probed with antibodies recognizing MMP2 and β-actin (all from Cell Signaling Technology, MA, USA) overnight at 4 °C.

To detect the apoptotic signaling proteins induced by PAK, A375 cells were treated with either 5 μM, 10 μM or 20 μM PAK for 72 h, harvested, and lysed in a RIPA buffer (Mention above). Subsequently, the total cell proteins were electrophoresed in a 10% SDS-PAGE followed by Western blot as described above. Cytochrome C, Cleaved Caspase-3, Cleaved Caspase-9 and β-actin were obtained from Cell Signaling Technology. The secondary antibodies were both horseradish peroxidase (HRP) conjugated goat anti rabbit IgG (GenScript, Nanjing, China). Signals were detected by chemiluminescence reagents (Beyotime Institute of Biotechnology, Shanghai, China) and imaged with a Tanon 5200 Imaging system (Shanghai, China).

2.7. Cellular uptake and internalization of PAK in A375 cells

20 μM of FITC-labeled proteins were used for intracellular uptake assays. To analyze the internalized efficiency of PAK, cells were incubated with FITC-labeled proteins at 37 °C for 48 h and harvested, and the cells were assessed using a FACSCalibur flow cytometer (BD Bioscience, San Jose, CA, USA). For analysis of intracellular uptake, cells were incubated with FITC-labeled proteins at 37 °C for 48 h, fixed with paraformaldehyde, and counterstained with DAPI (Beyotime Institute of Biotechnology, Shanghai, China) for the nucleus. Fluorescent images were observed with a confocal laser scanning microscope (CLSM, LSM800, Zeiss, Germany) and processed using the ZEN imaging software. To determine the effects of MMP2 on the activity of PAK, A375 cells were seeded in 6-well plates (50,000 cells/well) at 37 °C for 12 h and treated with MMP2 inhibitor SB-3CT at a final concentration of 1 μg/mL. PAK-FITC with a final concentration of 20 μM was added to the cells for 48 h. The medium was then discarded, and the cells were washed with HBBS three times, fixed with paraformaldehyde, and counterstained with DAPI for nucleus. The FITC fluorescence images were recorded with a fluorescence microscope (IX73, Olympus, Japan).

2.8. Mitochondrial membrane potential evaluation

A375 cells were seeded in 6-well plates at 50,000 cells per well at 37 °C for 12 h and treated with PAK at 20 μM for 72 h. Subsequently, the cells washed with HBSS, JC-1 (Beyotime Institute of Biotechnology, Shanghai, China), a potential sensitive dye, was added to a final concentration 10 μg/mL, and then the cells were incubated at 37 °C. After 30 min, the A375 cells were washed twice with HBBS. Excitation spectra at 525 nm (JC-1 monomers) and 595 nm (JC-1 aggregates) were analyzed using a confocal laser scanning microscope (CLSM, LSM800, Zeiss, Germany).

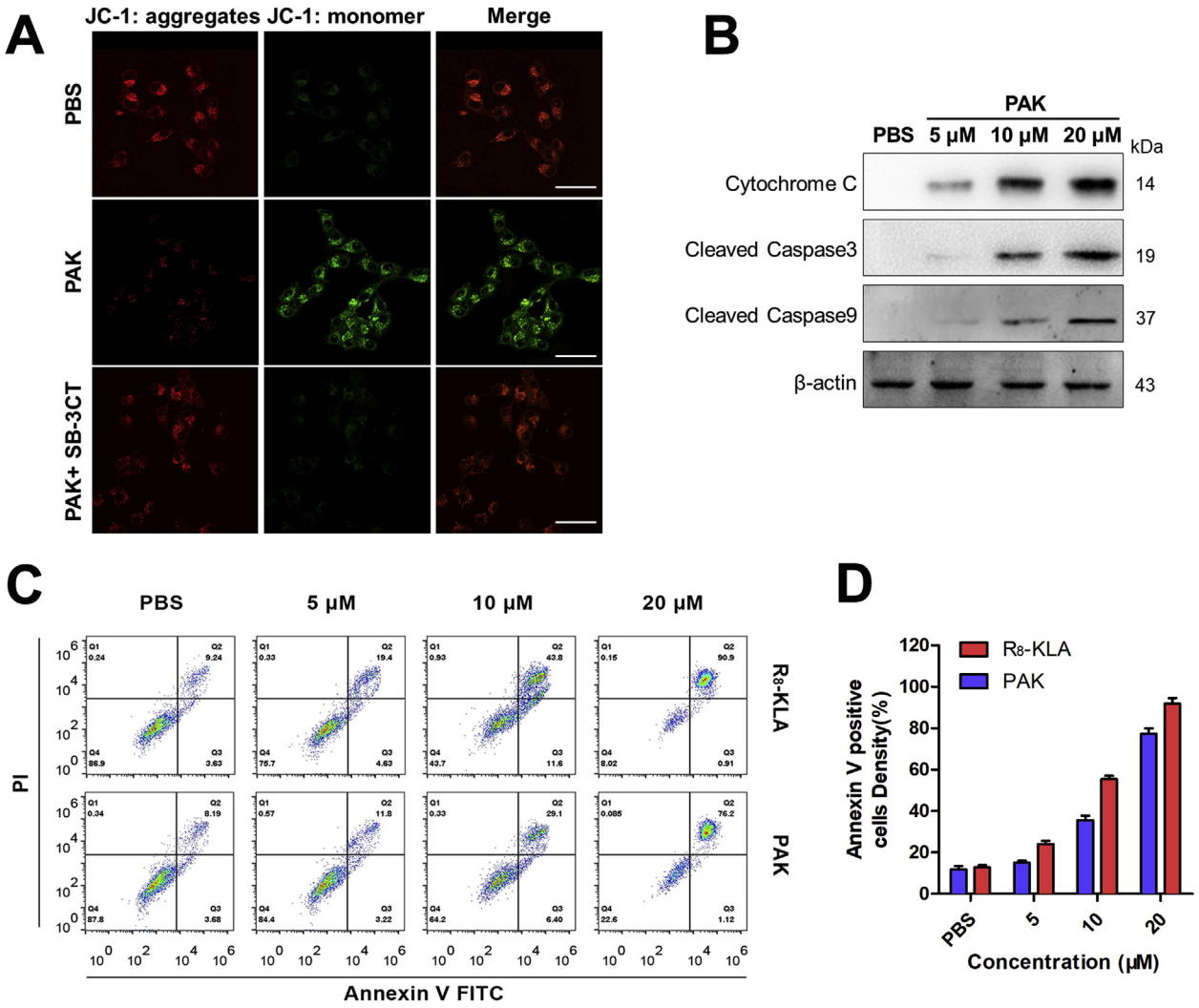

Fig. 7. PAK induced mitochondrial damage and cellular apoptosis.
(A) After pretreatment of SB-3CT, A375 cells were incubated with PAK (20 μM) for 48 h. Then, A375 cells were stained with JC-1 (Green: monomers, Red: aggregates). Scale bars, 50 μm. (B) Western blot analysis to detect the expression of Cytochrome C, Cleaved Caspase-3 and Cleaved Caspase-9 in A375 cells after PAK treatment. (C) A375 cells were treatment with R_8-KLA or PAK (5 μM, 10 μM and 20 μM), and level of apoptosis was measured by flow cytometry. (D) Relative cell densities of viable and apoptotic Annexin V positive cells were compared to untreated control cells. Data are mean ± SD of three independent experiments. . (For interpretation of the references to colour in this figure legend, the reader is referred to the Web version of this article.)

2.9. Hemolysis assay

Fresh blood was collected from BALB/c mouse in anticoagulant tubes contain EDTA.K_2. The blood sample was washed three time with HBSS and diluted to 2% (v/v) RBC suspension. Various concentration of R_8-KLA and PAK were incubated with RBC suspension at 37 °C for 1 h. Then, the supernatant was prepared by centrifugation at 1000 × *g* for 5 min and the release of hemoglobin was analyzed at 540 nm using a microplate reader (Thermo Fisher, Massachusetts, USA). The RBC suspension was incubated with 1% (v/v) Triton X-100 as the positive control, and the absorption of hemoglobin was set to 100%.

2.10. Animals and tumor xenograft model

All animal care and experimental protocols complied with the Laboratory Animal Management Regulations in China and the ethical committee at China Pharmaceutical University. All animals were used in accordance with the procedures approved by the Beijing Vital River Laboratory Animal Technology Inc. and Use Committee (license No. SCXK (su) 2016-0003). Animal studies are reported in compliance with the ARRIVE guidelines [35]. The tumor xenograft model was generated by subcutaneous injection of A375 cells (5×10^6 cells per mouse) in the right flanks of 6-week-old BALB/c nu/nu mice.

2.11. Pharmacokinetic study of PAK

Female BALB/c mice (n = 5) were treated with PAK (1 μmol/kg) intravenously via the tail-vein. At 0.25 h, 0.5 h, 1 h, 2 h, 4 h, 8 h, 24 h, and 48 h post injection, a blood sample was obtained from the eye socket vein in mice. The sera concentrations of PAK were measured with a His-Tag ELISA Detection Kit (L00436; GenScript, Nanjing, China). Serum drug data were analyzed with PKSolver (China Pharmaceutical University, Nanjing, China) [36].

2.12. In vivo fluorescence imaging of protein accumulation in tumors in animal models

When the tumor size reached about 200 mm^3, 20 nmol of Cy5-labeled proteins was injected intravenously through the tail vein. Mice were anaesthetized by intraperitoneal injection of chloral hydrate. Fluorescence imaging was performed using the IVIS imaging Spectrum System and analyzed with IVIS Living Imaging 3.0 software. After

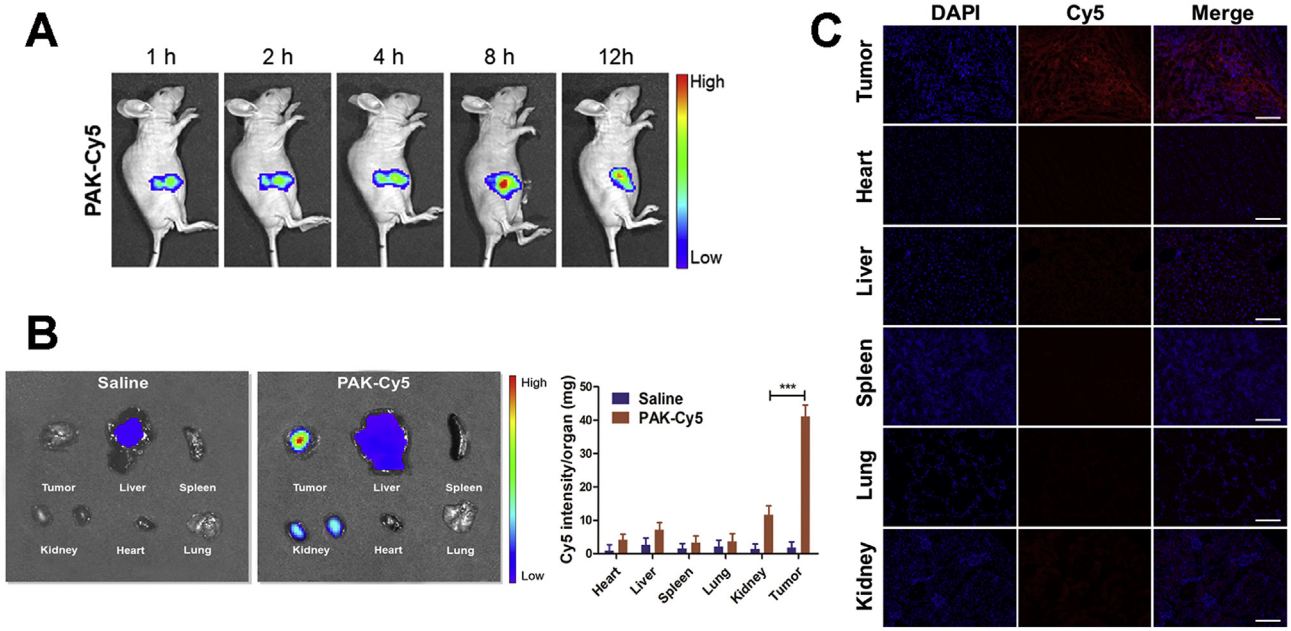

Fig. 8. *In vivo* NIR fluorescence images.
(A) Cy5-labeled PAK were intravenously administered into A375 tumor-bearing mice. *In vivo* NIR fluorescence images were obtained at different time points. (B) Tumor tissue and major organs (brain, heart, lung, liver, kidney, and spleen) from A375 xenograft-bearing mice were collected at 8 h after receiving the PAK-Cy5 injection. The organs were weighted and measured for Cy5 fluorescence. Data are mean ± SD (n = 3). $^{***}P < 0.001$. (C) Histologic sections of tumor tissue and major organs were obtained and recorded with a fluorescence microscope. The cell nuclei were stained with DAPI (blue). Scale bars, 100 μm. . (For interpretation of the references to colour in this figure legend, the reader is referred to the Web version of this article.)

imaging, tumors and vital organs (heart, liver, spleen, lung, and kidney) were isolated for frozen tissue sections, and counterstained with DAPI for the nucleus. Subsequently, these tissue sections were observed under an Olympus fluorescence microscope (IX73, Olympus, Japan).

2.13. *In vivo* antitumor effects of PAK

When the tumor size reached approximately 100 mm^3, mice (n = 20) were randomly divided into 4 groups (n = 5 per group) and treated with Saline, Cisplatin (5 mg/kg, every week), R_8-KLA (1 μmol/kg, every 3 days), and PAK (1 μmol/kg, every 3 days) by intraperitoneal injection. Before each administration, the tumor volumes were measured with a digital caliper and calculated according to the formula: tumor volume (mm^3) = 0.5 × (length of the tumor) × (width of the tumor)^2. Body weights of mice were recorded every day during the treatment to evaluate the systemic toxicity.

The tumors were obtained at the end of treatment, and frozen tissue sections were prepared for TUNEL staining. Meanwhile, the vital organs (heart, liver, spleen, lung, and kidney) were isolated and stained with H &E for histological analysis. Additionally, blood was collected to assay liver enzymes and hematological parameters by Servicebio Inc. (Nanjing, China).

2.14. *Statistical analysis*

Data are expressed as the mean ± SD. All statistical analyses were performed using ORIGIN 9.0 (OriginLab Corporation, Northampton, MA, USA) and GRAPHPAD PRISM 5 (GraphPad Software Inc., San Diego, CA, USA). The statistical analysis was determined using one-way ANOVA and Student's t-test. $^{***}P < 0.001$, $^{**}P < 0.01$, and $^{*}P < 0.05$ was considered significant.

3. Results

3.1. *Expression in E. coli, purification, and characterization of recombinant PAK*

To design a particularly expressible multifunctional protein, a PsTag polypeptide of 216 amino acids was fused through a neutralizing part of CPP (polyglutamic acid chain of 8 amino acids), followed by a cleavage sequence of MMP2 and a cationic CPP (polyarginine R_8), to the pro-apoptotic peptide KLA (Fig. 1). In addition, the specific cleavage sequence (PLGLAG) we chose for MMP2 was a site that had low cleavage activation by nontumor proteases [25,37]. A single cysteine at the C-terminus of this multifunctional protein served as the coupling site for thiol-based labeling, which could be used not only to label the fluorescent probe but also to label other functional molecules for further development. The amino acid sequences of PAK and two other control molecules we designed were shown in Table 1.

Due to the shielding effect of PsTag polypeptides, the fusion proteins could be expressed in *E. coli*, with undetectable production of inclusion bodies, and were purified by two-column chromatography steps. The PsTag fusion proteins showed relatively slow electrophoretic migration in SDS-PAGE (Fig. 2A) and Western blot (Fig. 2B) with SDS-PAGE molecular weights of about 60 kDa instead of the expected 24.6 kDa. This behavior revealed reduced binding of SDS, consistent with the previous study [17,19,38]. The purities of products were determined by RP-HPLC (Fig. 2C). Both profiles exhibited a single homogenous peak, validating the monodisperse character of each protein product. The secondary structures of fusion proteins were measured by CD, and the corresponding waveforms exhibited a remarkably negative minimum at 198 nm, characteristic of an unfolded polypeptide with random coils in the secondary structure (Fig. 2D). Mass spectrometry (Fig. 2E) revealed a single homogenous peak of the expected mass (24630.1 Da measured vs. 24636.2 Da). However, mass spectrometry of the PEGylated protein typically yielded a broader peak, on account of the heterogeneity of PEG polymers. To further determine the effect of the PsTag on the apparent molecular weight, the fusion proteins were detected by SEC-

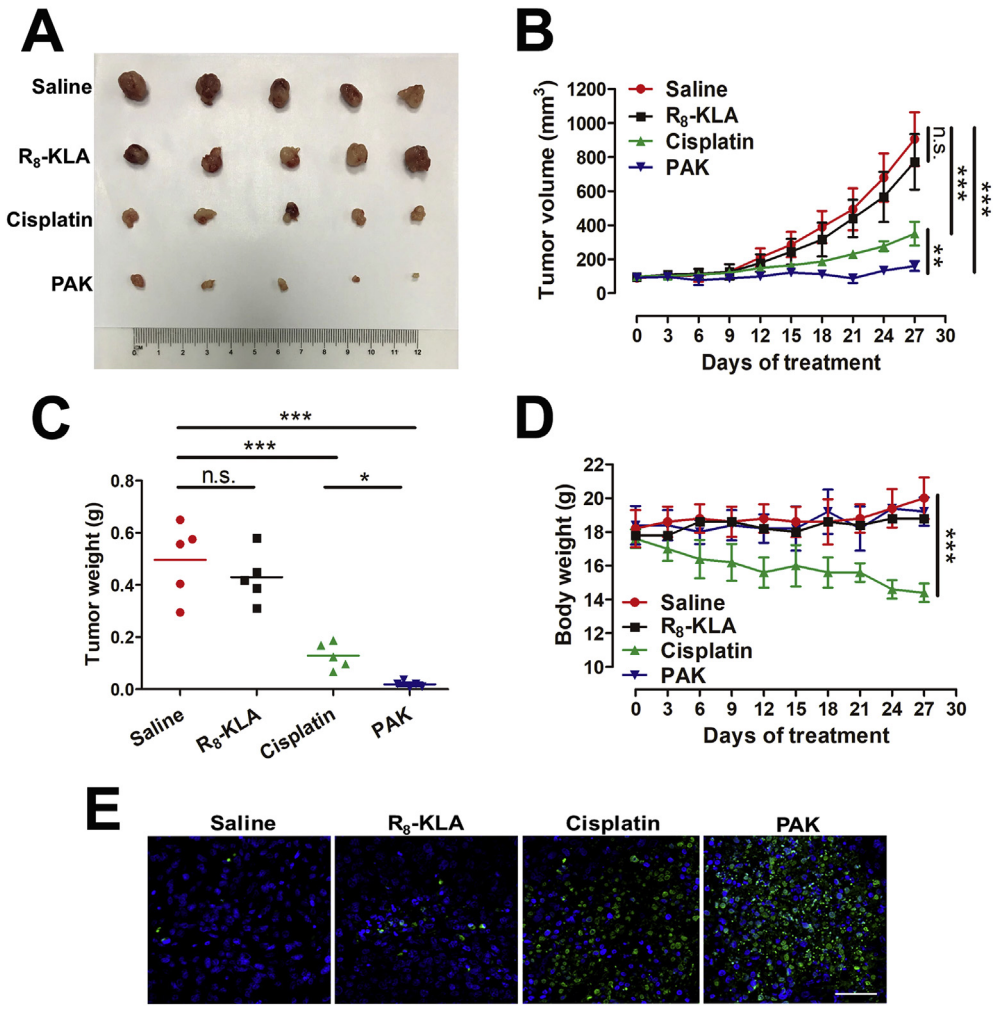

Fig. 9. *In vivo* evaluation of efficacy of PAK.
(A) On the 27th day after treatment, the tumors were obtained and the images of them were taken. (B) During the treatment period, tumor volumes were measured every three days. Data are mean ± SD (n = 5). (C) Tumor weights at the end of treatment. Horizontal bars represent mean values. (D) Body weights were measured every three days during the treatment period. Data are mean ± SD (n = 5). (E) Frozen tumor tissues sections were performed with TUNEL assay. Scale bars, 50 μm*$P < 0.05$; **$P < 0.01$; ***$P < 0.001$; *n.s.*, not significant.

HPLC (Fig. 2F). Referring to the standard curve (Fig. S1), we found that the apparent molecular mass of PAK was 108.6 kDa, larger than its actual 24.6 kDa. The PAK in aqueous solution had an average hydrodynamic diameter of 4.8 ± 0.2 nm (Fig. S2). This finding was typical for PsTag fusion proteins and could be explained by an extended and unstructured conformation, which made PsTag fusion proteins appear as larger molecules in SEC-HPLC [39]. In addition, to investigate the proteolytic protection effect of PsTag, PAK was evaluated in *vitro* by incubation with serum, showing resistance to serum proteases for at least 24 h at 37 °C (Fig. 2G and Figs. S3–4). As expected, R_8-KLA had low stability in serum (10% of R_8-KLA remaining at 24 h) (Fig. 2G and Fig. S3). On the other hand, PAK was stable up to 72 h after incubation (Fig. S5). Most peptides have short *in vivo* $t_{1/2}$ (2–30 min) owing to fast renal clearance and enzymatic degradation by proteases [9]. Similar to PEG, PsTag polypeptides also increased the *in vivo* $t_{1/2}$ of R_8-KLA to 5.05 ± 0.26 h by means of a shielding mechanism (Fig. 2H). R_8-KLA showed very strong hemolytic properties, while PAK exhibited much reduced hemolytic activity (Fig. 2I). To test the immunogenicity of this fusion protein, mice were injected with PAK and R_8-KLA every two days for 20 days. The IgG antibody titers specific for corresponding proteins were measured for each mouse, two weeks after the last immunization (Fig. 3A and B). Not surprisingly, all mice injected with R_8-KLA generated powerful immune responses independent of adjuvant coadministration. In contrast, PAK showed a remarkably reduced immunogenicity. Furthermore, production of early innate cytokines tumor necrosis factor (TNF)-α, interleukin (IL)-1β and IL-6 in primary human peripheral blood mononuclear cells (PBMCs) after incubation with PAK or R_8-KLA. Unlike PAK, R_8-KLA could trigger cytokine responses, compared with the negative control (PBS) (Fig. 3C). These data indicated that our protein was not strongly immunogenic.

3.2. Enzymatic digestion of PAK by MMP2

To better expound the design strategy and confirm the functionality of the cleavage site, the cleavage assessments were implemented by the enzymatic digestion with pretreatment of active MMP2. After treatment with MMP2 at various time points for up to 8 h, the enzyme-digested products were monitored by Urea-SDS-PAGE, and we observed that PAK could be digested completely after 4 h at 37 °C (Fig. S6). Comparing PAK to PK (uncleavable control), a new band emerged at the same location as the R_8-KLA peptide in the PAK lane (Fig. 4A). To further verify the MMP2-responsiveness, the digestion products were monitored by RP-HPLC and mass spectrometry. The peak of PAK completely disappeared, while new peaks emerged at a location similar to the R_8-KLA peptide when PAK was treated with 0.2 ng/μL MMP2 (Fig. 4B). The mass of the digestion products released from PAK was

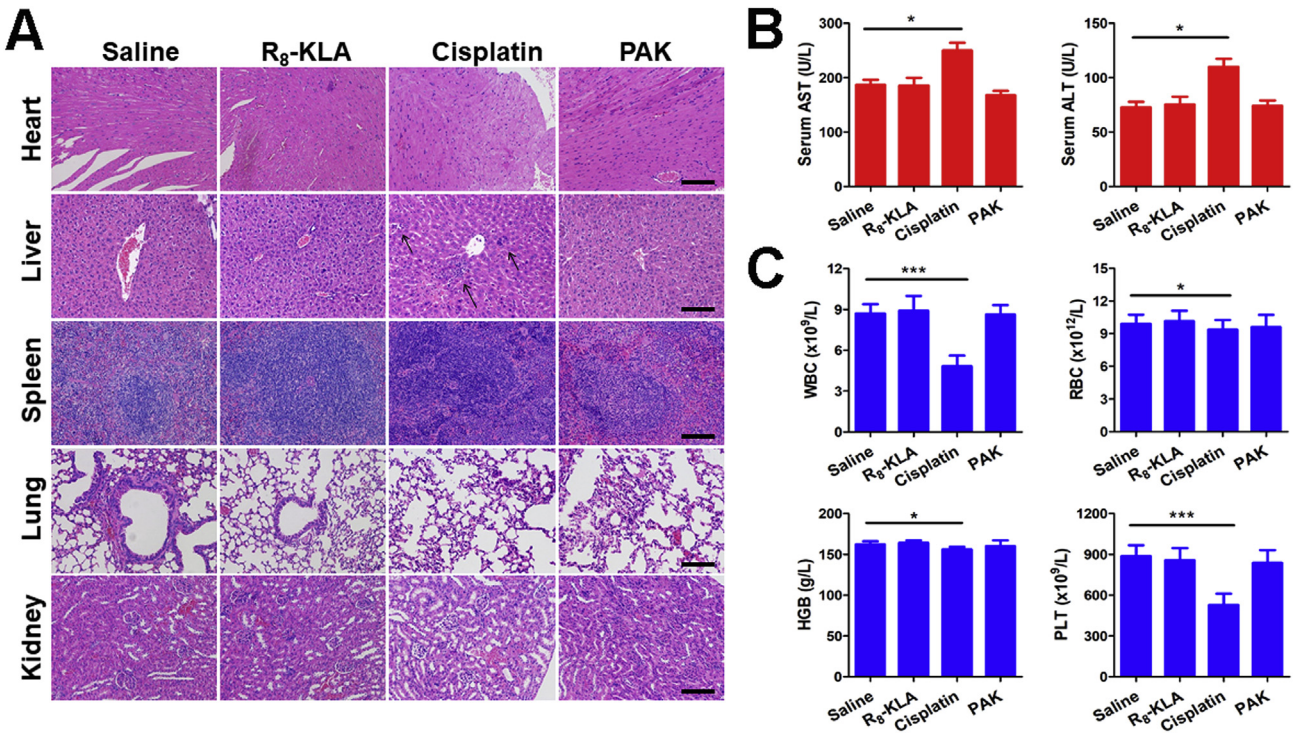

Fig. 10. *In vivo* evaluation of potential system toxicity of PAK.
(A) The vital tissues or organs (heart, liver, spleen, lung, and kidney) were obtained and assessed by H&E staining. Blood was analyzed for (B) AST & ALT levels and (C) hematological parameters. Data are mean ± SD (n = 5). *$P < 0.05$; ***$P < 0.001$; *n.s.*, not significant.

3346 Da instead of the controlled R_8-KLA 3104 Da (Fig. 4C). The extra 242 Da was likely due to the three amino acid residues, -LAG-, remaining from the substrate -PLGLAG-after MMP-2 digesting. Fig. 4 clearly showed that the MMP2-cleavable protein did not lose its "cleavability" after fusion with both PsTag and R_8-KLA at its two ends.

3.3. *In vitro cytotoxicity of PAK*

To assess the ability of PAK to exert selective cytotoxicity in normal cells and tumor cells, protein expression levels of MMP2 were examined first in cultured A375, HepG2, MCF7, BGC823 and L02 cell lines. Unlike in the L02 cell lines, the MMP2 protein was overexpressed in the cancer cell lines (Fig. 5A). Then, we detected the cytotoxic effects of PsTag and PAK *in vitro* using the CCK-8 assay. As shown in Fig. S7, the PsTag polypeptide had no significant cytotoxicity at a low concentration of 0.4 μM or even at a higher concentration of 50 μM against various cells. PAK inhibited the viability of the cancer cells in a time- and dose-dependent manner (Fig. S8 and Fig. 5B). The IC_{50} values of PAK ranged from 11 to 25 μM among these four cancer cell lines, similar to those of R_8-KLA (Fig. 5B). However, the L02 cells, which showed low expression of MMP2, were tolerant to cytotoxicity by PAK at the same concentrations. In addition, treatment with PAK produced cytotoxic effect in multiple tumor cells, whereas PK alone did not (Fig. 5B). The IC_{50} of these molecules against various cell lines was shown in Table 2.

Moreover, pretreatment of A375 cells with SB-3CT, a potent and selective inhibitor of MMP2, inhibited the cytotoxicity by PAK (Fig. 5C). On the other hand, after digestion with MMP2, the digested products of PAK induced a cytotoxic effect in L02 cells, and the level was similar to R_8-KLA (Fig. 5D). These results further suggested that the cytotoxicity of PAK was selectively activated by MMP2.

3.4. *MMP2-dependent cellular uptake*

To evaluate the internalization efficiency of this multifunctional protein, A375 cells and L02 cells were incubated with the PAK fusion protein which was labeled with maleimide- FITC dye at the single cysteine, and then analyzed by flow cytometry. The MMP2- cleavable protein demonstrated the potent cellular uptake in A375 cells (Fig. 6A). On the other hand, less uptake efficiency was observed in L02 cells (Fig. 6A). Confocal imaging exhibited that the R_8-KLA-FITC domain was efficiently internalized into A375 cells (Fig. 6B). Similar results were observed in MCF-7 cells (Fig. S9). Moreover, pretreatment of A375 cells with SB-3CT inhibited the internalization of PAK to A375 cells (Fig. 6C). Similarly, intracellular PAK was barely observed when A375 cells were cooled to 4 °C (Fig. 6C). The pretreatment of MMP2-responsive fusion protein with MMP2 eliminated the PsTag domain and the polyanionic sequence, exposed R_8, and increased the cellular uptake in L02 cells (Fig. S10). Thus, it can be summarized that PAK can realize potent KLA internalization by tumor cells in MMP2-rich environments. This protein reserved its "ability to be activated" after fusing with PsTag to form a macromolecule. After destroying the charge interaction and cleaving the linker simultaneously, this protein could release its masking domains to expose CPP.

3.5. *PAK induced mitochondrial damage and cellular apoptosis*

To measure whether PAK could induce injury of the mitochondrial membrane, we detected the mitochondrial membrane potential of the treated A375 cells through fluorescent probe JC-1. The results of fluorescence microscopy demonstrated that untreated A375 cells had strong red fluorescence (JC-1 aggregation) and weak green fluorescence (JC-1 monomer). As expected, the PAK-treated A375 cells exhibited a remarkable decrease in the red fluorescence and enhanced green fluorescence signals due to obvious injury of the mitochondrial membrane (Fig. 7A). After pretreatment with SB-3CT, the PAK-treated A375 cells showed weak green fluorescence similar to untreated A375 cells.

KLA was considered to induce cell apoptosis by disrupting the mitochondrial membrane and activating proteins such as caspase-3 and caspase-9 [31,32]. We performed Western blot to verify the activation

of mitochondria-mediated apoptotic pathway. As shown in Fig. 7B, treatment of A375 cells with PAK led to the significant leakage of cytochrome c from the mitochondria and the cleavage of caspase-3 as well as cleavage of caspase-9 compared with the control group. These findings were further validated by a flow cytometry assay using the Annexin V-FITC/Propidium Iodide staining. After PAK or R_8-KLA treatment, the growth of the A375 cells was dramatically decreased in a concentration-dependent way and induced prominent apoptosis (Fig. 7C and D).

3.6. In vivo fluorescence imaging of PAK accumulation in tumor tissue

To further prove the ability of PAK in tumor accumulation, we detected its distribution *in vivo* with fluorescent imaging in mice bearing the A375 xenograft. Strong signals were monitored in the tumor sites of mice injected with Cy5 dye-labeled PAK 8 h after injection (Fig. 8A). *Ex vivo* analysis also revealed that a substantial amount of PAK was selectively localized to the tumor (Fig. 8B). The vital tissues were further observed by histologic section, and higher fluorescence intensity could be found in the tumor, which was consistent with *ex vivo* analysis (Fig. 8C). The results indicated that PAK could effectively accumulate in the tumor tissue and had a long half-life in plasma up to the accumulation to tumor tissue.

3.7. Antitumor effects of PAK

The antitumor effects of tumor targeting and microenvironment-responsive PAK were evaluated in mice bearing the A375 xenograft. Based on the pre-experiment data and literature reported, 1 μmol/kg dose of PAK was selected and administered every 3 days (Fig. S11) [30,34,40]. After 4 weeks of treatment, the tumor volumes of the PAK-treated group were remarkably inhibited compared to the cisplatin-treated group ($P < 0.01$), R_8-KLA-treated group ($P < 0.001$) and saline-treated group ($P < 0.001$) (Fig. 9A and B). In addition, the tumors were isolated at the end of treatment, and the tendency of tumor weights was consistent with tumor volumes (Fig. 9C). Except for the cisplatin-treated group, body weights were not remarkably changed among experimental groups during the treatment period (Fig. 9D). The constant weight loss after treatment of cisplatin indicated there was significant system toxicity *in vivo*. Histological examinations, after staining with H&E of dissected tumors from the PAK-treated mice exhibited the existence of extensive necrotic areas, indicating that PAK showed potent antitumor effects *in vivo* (Fig. S12). The number of TUNEL-positive apoptotic cells in tumor tissue treated with PAK was also remarkably increased, compared to those treated with saline and R_8-KLA (Fig. 9E), indicating that PAK remarkably induced tumor cell apoptosis *in vivo*. All mice in the experiment survived during the treatment period (data not shown).

One of the main problems of current antitumor treatments is the adverse effects on normal tissues. To study whether PAK induced side effects, blood and serum chemistries, and histopathological lesions were examined at the end of treatment. No apparent histological changes at vital tissues or organs were observed after treatment with PAK (Fig. 10A). However, inflammatory cell infiltration at the liver and renal tubular injury at the kidney were observed after treatment with cisplatin. Serum levels of alanine aminotransferase (ALT) and aspartate aminotransferase (AST) were detected at the end of treatment. Except for the cisplatin-treated group, there were no remarkable differences among treatment groups and serum ALT and AST levels were within the normal range (Fig. 10B), revealing no toxicity to the liver function. Besides, treatment with PAK did not change the hematological parameters, including red blood cell (RBC) count, white blood cell (WBC) count, platelet (PLT) count, and hemoglobin (HGB) count (Fig. 10C), which suggested that there was little influence on the myeloid function after PAK treatment. More importantly, the typical chemotherapy drug cisplatin caused many hepatitis, renal tubule necrosis and significant bone marrow suppression in mice [41,42]. By contrast, PAK potently inhibited tumor growth *in vivo* without adverse effects to the liver, kidney and bone marrow. Collectively, these results confirmed the therapeutic potential of PAK in cancer therapy.

4. Discussion

Although conjugation to PEG and albumin are effective strategies for peptides and proteins, the multifunctional protein-tagged system would complement these strategies by extending half-life and reducing side effects of anticancer peptides. Moreover, uptake of PEGylated drugs into solid tumors is promoted by the EPR of tumors resulting from poor structural integrity, leaky tumor blood vessels and lack of lymphatic vessels. This EPR effect facilitates the selective permeability and retention of macromolecules (larger than 40 kDa) in solid tumor tissues [43,44]. The PEGylated liposome-encapsulated form of doxorubicin (Doxil), which can reduce cardiac toxicity, is the first FDA-approved nano-drug [45]. Besides maintaining potency and EPR effect, our system has some advantages over traditional PEGylation and genetic fusion strategies. (1) Our products are homogeneous and can be easily purified and characterized. (2) The three-dimensional structure of the fusion partner HSA needs to be maintained [46]. Unlike HSA fusion peptides, PsTag itself is an unstructured polypeptide. (3) Because of "ability to be activated" of our fusion protein, we anticipate our activated peptide (< 3% the size of HSA conjugates) to be able to penetrate solid tumors efficiently [9]. (4) Owing to the design of polypeptide, our products are unable to induce an immunogenic response. (5) The problem of the steric hindrance of macromolecules is not exist in our microenvironment-responsive fusion protein. (6) Kidney vacuolar degeneration, which is easily caused by PEGylated drugs, is not observed in this study.

Moreover, the anti-cancer mechanism of PAK is summarized as follows: Once to be injected into the circulation, the macromolecules (larger than 40 kDa) can be accumulated in tumor tissue through the EPR effect [44]. The PLGLAG peptide sequence can be hydrolyzed by the overexpressed MMP2 in tumor tissue [47]. Then the R_8-KLA was released and internalized into tumor cells through the arginine-rich cell-penetrating peptide. When the KLA was successfully delivered into tumor cells, it can cause mitochondrial disruption by triggering mitochondrial outer membrane permeabilization and swelling, resulting in the generation of relatively high levels of reactive oxygen species (ROS) and release of cytochrome c [32,48]. This liberated cytochrome c recruits and activates caspase-9, which in turn activates the executioner caspases, caspase-3 and caspase-7 [49,50]. Therefore, the activated caspases kill the tumor cells by proteolysis of vital cellular substrates.

CPP-mediated internalization of proapoptotic peptides into cells is highly efficient and results in the cell cytotoxicity [30,51]. Nonetheless, it does not differentiate the cell types and nonselectively enters into the various cell types [52,53]. Therefore, when fused with CPP, proapoptotic peptides may cause undesirable side effects to the livers and kidneys by internalization into the cells during blood circulation. To solve these problems, another strategy is to fuse KLA directly to a targeting peptide ligand, which makes the fusion peptides homing to the tumor tissues [30,34]. Of course, this strategy can be a good solution to nonselective problems of KLA, but the entire molecule still has only a few dozen amino acids causing its half-life to be short. Moreover, numerous cationic peptides with anticancer activity can also cause hemolysis, which influence further development [54]. Intermittent $_D$ to $_L$ amino acid replacement is an approach for effective reduction of the peptide helicity as well as the hemolytic activity [55]. Similarly, the approaches that reduce the hemolytic activity of peptides and enhance their *in vivo* $t_{1/2}$ are still sought.

Although not clearly addressed in this study, we speculate that our strategy could potentially be applicable for tumor-targeted delivery of liposomes, proteins, imaging agents and small molecule drugs. Furthermore, PAK itself can be employed as a targeting ligand, after

being conjugated traditional chemotherapeutic drugs, for tumor-targeted delivery of drugs in cancer therapy. This should broaden the utility and scope of our system.

In conclusion, we presented a strategy for tumor-targeted peptide delivery through multifunctional protein-tagged peptide. It was shown that the microenvironment-responsive fusion protein achieved enhanced tumor accumulation and pharmacokinetics and could inhibit tumor growth after cellular internalization of the anticancer peptide. This unusual potency was complemented by expanded hydrodynamic radius, minimal hemolytic activity, low immunogenicity, stability in mammalian serum, and simple use by fusing with a peptide of interest. The PAK fusion protein developed in this study was a promising, tumor targeting and microenvironment-responsive proapoptotic drug for cancer therapy. Nevertheless, meticulous work is needed for future research to acquire a clear understanding of the universality of this strategy.

Conflicts of interest

The authors declare that they have no conflicts of interest.

Acknowledgements

This research was supported by the National Natural Science Foundation of China (No. 81430082, 81703402), the National Science and Technology Major Project (2018ZX09201001-003-002), the Project funded by China Postdoctoral Science Foundation (2017M611957), the Fundamental Research Funds for the Central Universities (2015XPT02), A Project Funded by the Priority Academic Program Development of Jiangsu Higher Education Institutions, the “111 Project” from the Ministry of Education of China and the State Administration of Foreign Experts Affairs of China (No. 111-2-07), the Innovation Team of the “Double-First Class” Disciplines (CPU2018GF08).

Appendix A. Supplementary data

Supplementary data to this article can be found online at https://doi.org/10.1016/j.canlet.2019.03.016.

References

[1] K. Fosgerau, T. Hoffmann, Peptide therapeutics: current status and future directions, Drug Discov. Today 20 (2015) 122–128.
[2] A. Ellert-Miklaszewska, K. Poleszak, B. Kaminska, Short peptides interfering with signaling pathways as new therapeutic tools for cancer treatment, Future Med. Chem. 9 (2017) 199–221.
[3] X. Wang, Y. Qiao, I.A. Asangani, B. Ateeq, A. Poliakov, M. Cieå›Lik, S. Pitchiaya, C. Bvsk, X. Cao, X. Jing, Development of peptidomimetic inhibitors of the ERG gene fusion product in prostate cancer, Cancer Cell 31 (2017) 532–548.
[4] R. Drazen, R. Jung Su, Cell-penetrating peptides: strategies for anticancer treatment, Trends Mol. Med. 21 (2015) 560–570.
[5] B.E. Haug, K.A. Camilio, L.T. Eliassen, W. Stensen, J.S. Svendsen, K. Berg, B. Mortensen, G. Serin, J.F. Mirjolet, F. Bichat, Discovery of a 9-mer cationic peptide (LTX-315) as a potential first in class oncolytic peptide, J. Med. Chem. 59 (2016).
[6] D. Wu, Y. Gao, Y. Qi, L. Chen, Y. Ma, Y. Li, Peptide-based cancer therapy: opportunity and challenge, Cancer Lett. 351 (2014) 13–22.
[7] Y.F. Xiao, M.M. Jie, B.S. Li, C.J. Hu, R. Xie, B. Tang, S.M. Yang, Peptide-based treatment: a promising cancer therapy, J. Immunol. Res. (2015) 1–13 (2015-10-19) 2015 (2015).
[8] S. Marqus, E. Pirogova, T.J. Piva, Evaluation of the use of therapeutic peptides for cancer treatment, J. Biomed. Sci. 24 (2017) 21.
[9] S.C. Penchala, M.R. Miller, A. Pal, J. Dong, N.R. Madadi, J. Xie, H. Joo, J. Tsai, P. Batoon, V. Samoshin, A biomimetic approach for enhancing the in vivo half-life of peptides, Nat. Chem. Biol. 11 (2015) 793–798.
[10] E. Ezan, Pharmacokinetic studies of protein drugs: past, present and future, Adv. Drug Deliv. Rev. 65 (2013) 1065–1073.
[11] G. Pasut, F.M. Veronese, State of the art in PEGylation: the great versatility achieved after forty years of research, J. Control. Release 161 (2012) 461–472.
[12] J. Xia, Z. Wang, D. Huang, Y. Yan, Y. Li, J. Guan, Asymmetric biodegradable microdevices for cell-borne drug delivery, ACS Appl. Mater. Interfaces 7 (2015) 6293–6299.
[13] L. Zhang, M. Liu, S. Jamil, R. Han, G. Xu, Y. Ni, PEGylation and pharmacological characterization of a potential anti-tumor drug, an engineered arginine deiminase originated from Pseudomonas plecoglossicida, Cancer Lett. 357 (2015) 346–354.
[14] J.S. Suk, Q. Xu, N. Kim, J. Hanes, L.M. Ensign, PEGylation as a strategy for improving nanoparticle-based drug and gene delivery, Adv. Drug Deliv. Rev. 99 (2016) 28–51.
[15] K. Knop, R. Hoogenboom, D. Fischer, U.S. Schubert, Poly (ethylene glycol) in drug delivery: pros and cons as well as potential alternatives, Angew. Chem. Int. Ed. 49 (2010) 6288–6308.
[16] P.L. Turecek, M.J. Bossard, F. Schoetens, I.A. Ivens, PEGylation of biopharmaceuticals: a review of chemistry and nonclinical safety information of approved drugs, J. Pharm. Sci. 105 (2016) 460–475.
[17] J. Yin, L. Bao, T. Hong, Q. Wang, X. Gao, W. Yao, Genetic fusion of human FGF21 to a synthetic polypeptide improves pharmacokinetics and pharmacodynamics in a mouse model of obesity, Br. J. Pharmacol. 173 (2016) 2208–2223.
[18] J. Yin, L. Bao, R. Chen, W. Gao, X. Gao, W. Yao, Enhanced expression and distinctive characterization of a long-acting FGF21 and its potential to alleviate non-alcoholic steatohepatitis, Biochimie 151 (2018) 166–175.
[19] V. Schellenberger, C.-w. Wang, N.C. Geething, B.J. Spink, A. Campbell, W. To, M.D. Scholle, Y. Yin, Y. Yao, O. Bogin, A recombinant polypeptide extends the in vivo half-life of peptides and proteins in a tunable manner, Nat. Biotechnol. 27 (2009) 1186–1190.
[20] L. Hui, Y. Chen, Tumor microenvironment: sanctuary of the devil, Cancer Lett. 368 (2015) 7–13.
[21] W. T, D. Y, Tumor microenvironment and therapeutic response, Cancer Lett. 387 (2016).
[22] S.L. Wood, M. Pernemalm, P. Crosbie, A.D. Whetton, The role of the tumor-microenvironment in lung cancer-metastasis and its relationship to potential therapeutic targets, Cancer Treat Rev. 40 (2014) 558–566.
[23] T. Ji, Y. Zhao, Y. Ding, G. Nie, Using functional nanomaterials to target and regulate the tumor microenvironment: diagnostic and therapeutic applications, Adv. Mater. 25 (2013) 3508–3525.
[24] E.I. Deryugina, J.P. Quigley, Tumor angiogenesis: MMP-mediated induction of intravasation- and metastasis-sustaining neovasculature, Matrix Biol. 44–46 (2015) 94.
[25] H.X. Wang, X.Z. Yang, C.Y. Sun, C.Q. Mao, Y.H. Zhu, J. Wang, Matrix metalloproteinase 2-responsive micelle for siRNA delivery, Biomaterials 35 (2014) 7622.
[26] K. Kessenbrock, V. Plaks, Z. Werb, Matrix metalloproteinases: regulators of the tumor microenvironment, Cell 141 (2010) 52–67.
[27] L. Zhu, P. Kate, V.P. Torchilin, Matrix metalloprotease 2-responsive multifunctional liposomal nanocarrier for enhanced tumor targeting, ACS Nano 6 (2012) 3491–3498.
[28] S. Huang, K. Shao, Y. Kuang, Y. Liu, J. Li, S. An, Y. Guo, H. Ma, X. He, C. Jiang, Tumor targeting and microenvironment-responsive nanoparticles for gene delivery, Biomaterials 34 (2013) 5294–5302.
[29] L. Zhu, F. Perche, T. Wang, V.P. Torchilin, Matrix metalloproteinase 2-sensitive multifunctional polymeric micelles for tumor-specific co-delivery of siRNA and hydrophobic drugs, Biomaterials 35 (2014) 4213–4222.
[30] H.K. Jung, S. Kim, R.W. Park, J.Y. Park, I.S. Kim, B. Lee, Bladder tumor-targeted delivery of pro-apoptotic peptide for cancer therapy, J. Control. Release 235 (2016) 259–267.
[31] H.Y. Kim, S. Kim, H. Youn, J.K. Chung, H.S. Dong, K. Lee, The cell penetrating ability of the proapoptotic peptide, KLAKLAKKLAKLAK fused to the N-terminal protein transduction domain of translationally controlled tumor protein, MIIYRDLISH, Biomaterials 32 (2011) 5262–5268.
[32] H.M. Ellerby, W. Arap, L.M. Ellerby, R. Kain, R. Andrusiak, G.D. Rio, S. Krajewski, C.R. Lombardo, R. Rao, E. Ruoslahti, Anti-cancer activity of targeted pro-apoptotic peptides, Nat. Med. 5 (1999) 1032–1038.
[33] B. Law, L. Quinti, Y. Choi, R. Weissleder, C. Tung, A mitochondrial targeted fusion peptide exhibits remarkable cytotoxicity, Mol. Canc. Therapeut. 5 (2006) 1944–1949.
[34] B. Fu, W. Long, Y. Zhang, A. Zhang, F. Miao, Y. Shen, N. Pan, G. Gan, F. Nie, Y. He, Enhanced antitumor effects of the BRBP1 compound peptide BRBP1-TAT-KLA on human brain metastatic breast cancer, Sci. Rep. 5 (2015) 8029.
[35] C. Kilkenny, W. Browne, I.C. Cuthill, M. Emerson, D.G. Altman, Animal research: reporting in vivo experiments: the ARRIVE guidelines, J. Gene Med. 12 (2010) 561–563.
[36] Y. Zhang, M. Huo, J. Zhou, S. Xie, PKSolver: an add-in program for pharmacokinetic and pharmacodynamic data analysis in Microsoft Excel, Comput. Methods Progr. Biomed. 99 (2010) 306–314.
[37] H. Li, S.S. Yu, M. Miteva, C.E. Nelson, T.A. Werfel, T.D. Giorgio, C.L. Duvall, Matrix metalloproteinase responsive, proximity-activated polymeric nanoparticles for siRNA delivery, Adv. Funct. Mater. 23 (2013) 3040–3052.
[38] M. Schlapschy, U. Binder, C. Börger, I. Theobald, K. Wachinger, S. Kisling, D. Haller, A. Skerra, PASylation: a biological alternative to PEGylation for extending the plasma half-life of pharmaceutically active proteins, Protein Eng. Des. Sel. 26 (2013) 489–501.
[39] W. Gao, J. Yin, L. Bao, Q. Wang, S. Hou, Y. Yue, W. Yao, X. Gao, Engineering extracellular expression systems in Escherichia coli based on transcriptome analysis and cell growth state, ACS Synth. Biol. 7 (2018) 1291–1302.
[40] V. Sarangthem, Y. Kim, T.D. Singh, B. Seo, S. Cheon, Y. Lee, B. Lee, R. Park, Multivalent targeting based delivery of therapeutic peptide using AP1-ELP carrier for effective cancer therapy, Theranostics 6 (2016) 2235–2249.
[41] S. Dasari, P.B. Tchounwou, Cisplatin in cancer therapy: molecular mechanisms of action, Eur. J. Pharmacol. 740 (2014) 364–378.
[42] M. Demaria, M.N. Oleary, J. Chang, L. Shao, S. Liu, F. Alimirah, K. Koenig, C. Le, N. Mitin, A.M. Deal, Cellular senescence promotes adverse effects of chemotherapy

and cancer relapse, Cancer Discov. 7 (2017) 165–176.
[43] S. Taurin, H. Nehoff, K. Greish, Anticancer nanomedicine and tumor vascular permeability; where is the missing link? J. Control. Release 164 (2012) 265–275.
[44] J. Fang, H. Nakamura, H. Maeda, The EPR effect: unique features of tumor blood vessels for drug delivery, factors involved, and limitations and augmentation of the effect, Adv. Drug Deliv. Rev. 63 (2011) 136–151.
[45] Y. Barenholz, Doxil® — the first FDA-approved nano-drug: lessons learned, J. Control. Release 160 (2012) 117–134.
[46] M.T. Larsen, M. Kuhlmann, M.L. Hvam, K.A. Howard, Albumin-based drug delivery: harnessing nature to cure disease, Mol. Cell. Ther. 4 (2016) 3.
[47] T. Jiang, E.S. Olson, Q.T. Nguyen, M. Roy, P.A. Jennings, R.Y. Tsien, Tumor imaging by means of proteolytic activation of cell-penetrating peptides, Proc. Natl. Acad. Sci. U. S. A 101 (2004) 17867–17872.
[48] J.C. Mai, Z. Mi, S. Kim, B. Ng, P.D. Robbins, A proapoptotic peptide for the treatment of solid tumors, Cancer Res. 61 (2001) 7709–7712.
[49] P. Li, D. Nijhawan, I. Budihardjo, S.M. Srinivasula, M. Ahmad, E.S. Alnemri, X. Wang, Cytochrome c and dATP-dependent formation of apaf-1/caspase-9 complex initiates an apoptotic protease cascade, Cell 91 (1997) 479–489.
[50] X. Jiang, X. Wang, Cytochrome C-mediated apoptosis, Annu. Rev. Biochem. 73 (2003) 87–106.
[51] G. Guidotti, L. Brambilla, D. Rossi, Cell-penetrating peptides: from basic research to clinics, Trends Pharmacol. Sci. 38 (2017) 406–424.
[52] K. Mie, B. Ditlev, M.N. Hanne, Applications and challenges for use of cell-penetrating peptides as delivery vectors for peptide and protein cargos, Int. J. Mol. Sci. 17 (2016) 185.
[53] M. Rizzuti, M. Nizzardo, C. Zanetta, A. Ramirez, S. Corti, Therapeutic applications of the cell-penetrating HIV-1 Tat peptide, Drug Discov. Today Off. 20 (2015) 76–85.
[54] X. Liu, R. Cao, S. Wang, J. Jia, H. Fei, Amphipathicity determines different cytotoxic mechanisms of lysine- or arginine-rich cationic hydrophobic peptides in cancer cells, J. Med. Chem. 59 (2016) 5238–5247.
[55] N. Papo, A. Braunstein, Z. Eshhar, Y. Shai, Suppression of human prostate tumor growth in mice by a cytolytic d-, l-amino acid peptide membrane lysis, increased necrosis, and inhibition of prostate-specific antigen secretion, Cancer Res. 64 (2004) 5779–5786.